Model-based monitoring and control of industrial freeze-drying processes: Effect of batch nonuniformity

This is an electronic version (author's version) of an article published in DRYING TECHNOLOGY, Volume 28, Issue 5, pages 577-590 (2010).

DRYING TECHNOLOGY is available online at:

http://www.tandfonline.com/openurl?genre=article&issn=0737-3937&volume=28&issue=5&spage=577

Model-based monitoring and control of industrial freeze-drying processes: effect of batch non-uniformity

Antonello A. Barresi, Roberto Pisano, Valeria Rasetto, Davide Fissore*, Daniele L. Marchisio

Dipartimento di Scienza dei Materiali e Ingegneria Chimica,
Politecnico di Torino, corso Duca degli Abruzzi 24, 10129 Torino (Italy)

* Corresponding author
tel: +39-011-0904693
fax: +39-011-0904699
e-mail: davide.fissore@polito.it

Abstract

This paper deals with the monitoring and control of the freeze-drying of pharmaceuticals in vials taking into account batch heterogeneity. Firstly, the problem of non-uniformity of the batch is addressed: the vials in the chamber of the freeze-dryer can, in fact, exhibit different dynamics due not only to radiation from the wall of the chamber, but also to temperature gradients on the heating shelf, vapor fluid dynamics and non-uniform inert distribution, as it has been evidenced by means of *Computational Fluid Dynamics* simulations. Then, the effect of batch heterogeneity on the performance of the monitoring and control system is discussed, and a new tool is presented: it is based on an advanced algorithm, the *Dynamic Parameters Estimation*, that estimates the state of the system (product temperature and residual ice content) by using the results of the Pressure Rise Test, coupled with a controller (*LyoDriver*) that changes the shelf temperature in order to maintain product temperature below the maximum allowed value, thus minimizing the duration of primary drying.

Keywords

- Freeze-drying
- Product monitoring
- Batch heterogeneity
- CFD
- LyoDriver
- Dynamic Parameter Estimation

Introduction

Lyophilization is a drying process where water (or another solvent) is removed from a frozen product by sublimation, thus working at low temperature and low pressure: this makes the process suitable for heat-sensitive materials, e.g., pharmaceuticals. Moreover, the freeze-drying process can be carried out in a sterile environment, and warrants a final product that can be easily re-hydrated (Liapis and Bruttini, 1995; Liapis et al., 1996; Sadikoglu and Liapis, 1997).

The freeze-drying cycle is usually specified by means of a recipe, in terms of shelf temperature and chamber pressure over time: this recipe is usually obtained from an extended experimental campaign based on a trial-and-error procedure. However, this approach does not guarantee repeatable conditions for the freezing and sublimation steps; there can be, for example, changes from batch-to-batch due to stochastic sub-cooling phenomena, leading to different nucleation temperatures. Moreover, there may be further changes introduced by the operator, or caused by variations in the materials or in the operating conditions. Beside the highlighted factors, the small-scale equipment, used for recipe development, and the large-scale equipment, used in the industrial process, are different with respect to vapor fluid dynamics, temperature distribution over the shelves, heating/cooling capacity, and radiation effects: the result is that a product could be damaged when the recipe developed in a pilot-scale freeze-dryer is used in an industrial-size apparatus. Moreover, it could take much longer than needed to freeze-dry a certain product if the process is not well-designed and optimized (Tang and Pikal, 2004; Sadikoglu et al., 2006). According to recent Process Analytical Technology (PAT) guidelines, issued by US Food and Drugs Administration in 2004, the process has to be investigated in depth in order to develop in-line tools for better monitoring and controlling of the manufacturing process, with the scope of ensuring the final product quality.

This paper is focused on the investigation of the causes of batch heterogeneity, making use of experimental results and mathematical simulations: both a detailed mono-dimensional model, for describing the product evolution in vials, and Computational Fluid Dynamics (CFD), for describing the vapor fluid dynamics in the chamber, are employed to this purpose. Three steps are involved in the process: freezing, primary drying, during which the solvent is removed from the frozen product by sublimation, and, eventually, secondary drying, to remove the residual water from the partially dried cake. This work focuses on monitoring and control of primary drying for the freeze-drying of pharmaceuticals, as this is usually the

longest and most risky phase of the whole process. The case of lyophilization in vials is considered in details, but the methodology proposed here can be easily extended to other products in tray. The relevance of non-uniformity for process monitoring and control will be discussed, and, finally, possible modifications and performance of the presented monitoring and control algorithms will be discussed.

State of the art

Maximum product temperature and residual ice content (i.e., the position of the sublimation interface) are the key variables that should be monitored and controlled in a freeze-drying process: the former should be maintained below collapse (or melting) temperature, so as to avoid loss of macroscopic structure, while the latter gives the state of progression of drying. With traditional devices used to monitor a freeze-drying cycle (e.g., thermocouples, spectroscopy-based methods, pressure gauges, weighing balances) this information is not easily achievable, as the largest part of these sensors may allow to determine only the end of primary drying, and, at best, they provide measurements that are not representative of the whole batch: for these reasons they are not applicable in industrial environments. The state of the art of freeze-drying monitoring has been discussed in detail in previous papers (Galan et al., 2007; Barresi et al., 2009), where an innovative and modular monitoring system that takes advantage of redundancy and synergistic effect of different devices was presented.

Nowadays, most of the non-invasive monitoring tools use the Manometric Temperature Measurement (MTM) approach, which is based on the interpretation of the pressure rise curve due to shut-off of the valve placed between the drying chamber and the condenser (Pressure Rise Test, PRT): a discussion of the different approaches presented in the past, together with the description of an improved algorithm based on a dynamic model, called Dynamic Parameters Estimation (DPE), can be found in the work of Velardi et al. (2008). This technique allows to obtain a full-state estimation of the system, but gives only an average state of the system, without taking into account batch unevenness caused, for instance, by radiation or temperature gradients on the heating shelves. In fact, model-based monitoring tools developed after the MTM approach assume that the batch is homogeneous, but since the unevenness can be relevant during the process and, in particular, nearby the end-point of the primary drying, they are not able to give reliable results throughout all the sublimation step. Moreover, they generally fail in the presence of a significant contribution to heating by

radiation, as this modifies the expected temperature profile in the product.

Poor process control is a limitation of the current technology: control actions are often based on empirical information coming from previous experimental runs carried out with the same product, while even the most advanced industrial freeze-dryers are equipped with control systems that are simply data collectors for certain key variables, beside maintaining chamber pressure and shelf temperature at the values indicated by the user (Liapis et. al, 1996). Fissore et al. (2008) presented an ideal model-based control that manipulates the shelf temperature in order to maintain the product temperature at a safe level, and proposed, in particular, a proportional controller manipulating the temperature of the heating fluid according to the system state estimation obtained through a Kalman filter based observer; the possibility to manipulate the chamber pressure was also considered.

According to the literature, it has been recently shown that an in-line adaptive control procedure aiming to minimize the drying time is feasible. Tang et al. (2005) and Pikal et al. (2005) proposed, and patented, an expert system, named SMART^{TM} Freeze-Dryer, for manipulating the shelf temperature and the chamber pressure using the results obtained by means of MTM (Milton et al., 1997). Gieseler et al. (2007) validated experimentally the SMART^{TM} Freeze-Dryer with different type of excipients, formulations (involving crystalline and amorphous products) and vials: results confirm that the algorithm can be a useful tool for development of a lyophilization cycle during a single freeze-drying run. Nevertheless, it has no predictive capacity as it does not take into account the evolution of the product as a consequence of the actions taken and, thus, in our opinion a wide margin for optimization may exist. A similar approach has been proposed by Oetjen (1999) and by Oetjen and Haseley (2004), but it is based on the results given by the Barometric Temperature Measurement (BTM).

The problem of the heterogeneity of a batch, due to the intrinsic heterogeneity of the product, and to differences from vial to vial of the heat transfer rate and mass transfer resistance to vapor flow in the dried layer, is well known among the freeze-drying scientific community. Many factors contribute to produce significantly different heat transfer rates in the vials of a batch, such as the shape of the bottom of the vial, that affects the heat transfer from the fluid in the shelves to the product, the contact between the vials, and the radiation from the chamber walls and the chamber door. In particular, radiation effects from chamber walls represent a very well documented cause of inter-vial variance (Gan et al., 2004, 2005a, 2005b; Kobayashi et al., 1991; Oetjen and Haseley, 2004). As a matter of fact, the possibility of acting on the wall temperature in order to achieve higher uniformity in the batch has been

deeply investigated, and a system that controls the temperature of the chamber walls has also been patented (Sennhenn et al., 2005).

Beside the radiation effect, another significant cause of inter-vial variance is the fluid dynamics of the sublimating vapor inside the lyophilization chamber. Until now, this aspect has been neglected because of the inherent difficulties in recognizing it and in identifying and quantifying its effects on the experimental results. These effects can be efficiently investigated by means of CFD, that can nowadays be reliably used to investigated complex industrial processes. In particular, the effect of some geometrical parameters of the drying chamber (clearance between the shelves and position of the duct between the chamber and the condenser) on the fluid dynamics of the sublimated vapor in both a small scale (chamber volume of about 0.2 m^3) and an industrial scale drying chamber (chamber volume of about 10 m^3) has been investigated as a function of the sublimation rate by Rasetto et al. (2008b). The results highlight that the operating conditions (in particular the vapor pressure) inside the drying chamber are affected by the global fluid dynamics within the chamber itself. Typically, higher pressure values are observed in the centre of the shelves positioned far from the condenser duct, and the global pressure drop across each shelf increases if the clearance between the shelves is reduced. The pressure gradients inside the chamber are important because the product temperature depends on the pressure (i.e., the higher is the vapor pressure the higher is the product temperature) and, thus, they represent a cause of batch unevenness.

Experimental and modeling approaches

An extended experimental campaign has been carried out in our research lab in Politecnico di Torino by using a pilot-scale freeze-dryer (*LyoBeta* 25 by Telstar) having a chamber volume of about 0.2 m^3: the goal is to investigate the contribution of radiation from the chamber wall, and from other devices inserted in the chamber, to process dynamics (see also Rasetto et al., 2008a).

The effect of radiation from chamber walls has been investigated also by means of numerical simulations by using a detailed mathematical model of the process (Velardi and Barresi, 2008a) in order to compare the product temperature evolution of the edge-vials and of those placed in the core of the batch. Radiation from the chamber walls and the shelves surface has been modelled using the equations and the parameters given by Gan et al. (2005a, 2005b).

The effect of vapor fluid dynamics has been investigated by means of the commercial CFD code Fluent 6.3: the continuity and Navier-Stokes equations are solved by resorting to a finite-volume scheme. With this approach the governing equations are discretized on a computational grid constituted by a large number of small non-overlapping control volumes (i.e., computational cells). The three-dimensional simulations carried out in this work are based on structured computational grids of about 300,000 – 600,000 hexahedral cells, representing the geometry of the freeze-drying chamber. The computational grids were created by using the grid generator GAMBIT, and for all the investigated cases grid independence of the solution was verified by successive grid refinement. Steady-state simulations were carried out by considering the water vapor as a compressible fluid, whose density is evaluated according to the ideal gas law, whereas the viscosity is calculated with the standard kinetic theory for dilute gases. The Semi-Implicit Method for Pressure-Linked Equations (SIMPLE) algorithm was used to solve the pressure-velocity coupling, whereas in order to contrast the insidious effects of numerical diffusion the Quadratic Upwind Interpolation for Convective Kinematics (QUICK) was used, by refining an initial solution obtained with a first-order upwind interpolating scheme. Details concerning these numerical methods can be found in the book of Ferziger and Peric (2002). Very restrictive convergence criteria were used (normalized residuals smaller than 10^{-6}) and, in some cases, small under-relaxation factors needed to be used to reach convergence. In our simulations the inlet and the outlet boundary conditions were set for the sublimation surfaces and for the final section of the duct connecting the chamber to the condenser, respectively. As far as this latter surface is concerned a standard pressure-outlet boundary condition was used, where the outlet pressure was that super-imposed by the condenser. The sublimation surfaces, corresponding to the vials placed on each shelf, were described as mass-flow-inlet; it is important to point out here that the geometrical details of the vials over the shelves have not been considered: as a matter of fact, the layer of vials was modeled as a continuous slab with a thickness of 43 mm, corresponding to that of the vials partially closed by the stopper (of course, the fraction of surface corresponding to sublimating products has been taken into account to set the correct value of sublimation flux in the model). The sublimation rate can be easily correlated to the operating conditions (shelf temperature and chamber pressure) and to the vial and product characteristics by means of the following mass balance equation:

$$\frac{dm}{dt} = A\frac{p_{w,i} - p_{w,c}}{R_P + R_S}, \qquad (1)$$

coupled with an equation stating that the heat flow from the shelf to the product is used to

sublimate the ice:

$$\Delta H_s A \frac{p_{w,i} - p_{w,c}}{R_P + R_S} = A_v K_v \left(T_{shelf} - T_B \right), \quad (2)$$

where A is the internal cross surface section of the vial, A_v is the bottom surface of the vial, R_P and R_S are respectively the mass transfer resistance in the dried layer and in the stopper, and K_v is the heat transfer coefficient between the shelf and the bottom of the vial. If the operating conditions (T_{shelf} and $p_{w,c}$) and the parameters of the system (K_v, R_P, R_S, A, A_v) are known then Eq. (2) allows to calculate the equilibrium vapor pressure ($p_{w,i}$) at the interface of sublimation, and this value can be used to calculate the sublimation flux using Eq. (1). Solution of Eq. (2) requires the knowledge of the product temperature at the bottom of the vial (T_B): to this purpose, a correlation was given by Tang et al. (2005, 2006a, 2006b), who used a similar model to interpret the results of the pressure rise test for monitoring the primary drying. This simple model allows to predict the sublimation flux value in each point of the shelf and in each instant of time of the batch, depending to the local vapor pressure, shelf temperature and thickness of frozen layer. Preliminary results show that the local values of the operating conditions indeed affect the local sublimation flux, however, these differences are not strong enough to influence the global fluid dynamics of the chamber. Therefore in what follows results obtained super-imposing constant sublimation fluxes over the shelves (i.e., 0.1 – 1.0 kg m^{-2} h^{-1}) will be presented.

In order to investigate the effect of vapor fluid dynamics, and of other sources of heterogeneity, e.g. non-uniform shelf temperature and inert distribution, a detailed, one-dimensional model, previously validated (Velardi and Barresi, 2008a), is here used. The evolution of product temperature, that should not overcome an upper limit defined by the characteristics of the considered product, as well as that of the position of the sublimating interface, that indicates the progress of primary drying, have been calculated. As far as the modeling of the process in the vial is concerned, as a test case, simulations have been carried out by using the same parameters given in the work of Velardi and Barresi (2008a) for the properties of the freeze-dried product and for the heat and mass transfer coefficients: they refer to the freeze-drying of a 5% solution of bovine serum albumin, buffered with tris-HCl 0.1 M, in vials having a total volume of 4 ml, internal diameter of $14.25 \cdot 10^{-3}$ m, mean thickness of $1 \cdot 10^{-3}$ m, and maximum air gap at the bottom of $0.7 \cdot 10^{-3}$ m; the geometry of the chamber is the same of the large scale equipment previously described.

Results and discussion

1. Evaluating causes of batch heterogeneity

Figure 1 shows the results obtained during an experimental freeze-drying cycle: the product mass for each vial was measured before loading the freeze-dryer and after about 5 hours of vacuum in order to compare the sublimated solvent mass in vials placed in different locations of the batch and, thus, to understand how drying varies depending on vial position. As it can be expected, vials near the door and the chamber walls exhibit higher sublimation rate, due to the radiation flux. This behavior is typical of all small-scale equipment and has to be taken into account during the scale-up of the recipe to the industrial-scale apparatus.

Numerical simulations have also been used to assess the role of radiation in the same operating conditions of the experimental test shown in Figure 1. Figure 2 shows that when the edge-vials have completed primary drying, the other vials still have part of the frozen solvent not completely sublimated, in good qualitative agreement with the results shown in Figure 1.

In Figure 3 (l.h.s.) the pressure profiles over trays positioned at different elevation from the bottom are shown for two different cases (A and B) characterized by different clearances between the shelves (the clearance in Case B is higher than in Case A): both simulations were carried out super-imposing the same sublimation rate (i.e., 1.0 kg m^{-2} h^{-1}). Figure 3 (l.h.s.) shows that, in order to guarantee the same sublimation rate, the vapor in Case A has to experience higher pressure drops than in Case B; in fact, the number of shelves is higher and, thus, the total flow rate in the chamber. Moreover, the results reported in Figure 3 (l.h.s.) show the strong effect related to the position of the condenser duct: the pressure across each shelf decreases with the *y* coordinate when getting closer to the condenser duct (the coordinate system is shown in Figure 4, r.h.s.) and the minimum pressure value is observed over the shelves positioned closer to the condenser duct (13th in case A and 11th in case B).

The sublimation rate can be considered approximately constant during most of the primary drying phase, but when the thickness of the dried layer becomes larger than a critical value, toward the end of the sublimation, the sublimation rate assumes smaller values. Thus, in order to consider typical operating conditions throughout an entire batch, also smaller values for the sublimation rate were considered. In Figure 3 (r.h.s.) the pressure profiles over some shelves in the large-scale apparatus along the *x* coordinate are reported for different sublimation rates (i.e., 1.0 - 0.7 - 0.5 kg m^{-2} h^{-1}). As it can be observed, both the absolute pressure value and the pressure gradient over the trays decrease when the sublimation rate is

decreased; in all the cases represented, the pressure at the end of the duct has been set equal to 10 Pa: this allows to evaluate the effect of the value of sublimation flux on the pressure drop between the chamber and the condenser.

In Figure 4 the pressure gradients obtained by the CFD simulations for the small and the large scale apparatus when the clearance between the shelves is the same (equal to 100 mm), and the duct is positioned in the middle plane of the rear wall of the chamber, are compared. It can be observed that the clearance does not scale with the size of the apparatus and that if the load of the apparatus is increased by reducing the clearance, at the same time the pressure over the central part of the shelf is increased. Moreover, the clearance cannot be reduced below a minimum value in order to allow charging and discharging of the vials. The pressure drop increase is proportional to the square of the shelf characteristic dimension (because the sublimation flow increases with shelf size) and, thus, this effect is quite limited in the small apparatus. From these data it seems that in the laboratory scale apparatus the batch can be considered nearly uniform, but this is true only for the fluid dynamics aspects, while the radiation contribution from the chamber wall, as shown before, may be significant, and is much more relevant at this small scale.

Also the addition of an inert gas to control the pressure may have a significant influence not only on the fluid dynamics in the chamber but also on the local composition of the atmosphere, and thus on the local partial pressure of water: this can be an additional source of variability in the batch. To this purpose several simulations have been carried out considering different mass fluxes of inert. This aspect is very important especially for the laboratory scale apparatus, where the inert is typically introduced in the drying chamber only by one inlet. In Figure 5 the mass fraction of inert gas (N_2) is shown: in this simulation the average mass fraction of inert is 30 %, but all the inert gas is concentrated in the clearance between the gas inlet and the outlet of the chamber (duct). In Figure 5 the region where the inert mass fraction is higher than the half of the average value is shown (the inlet is positioned in the front side).

Finally, the non-uniform shelf temperature can be a relevant cause of non-uniform temperature evolution in the various vials of the batch. In fact, it is generally considered acceptable a maximum temperature difference of 2°C between two points of the shelf in an industrial-scale equipment, but up to 3°C are often observed in small-scale units. Of course also differences in filling volume between vials and in the positioning of the stopper, depending on the operation of the dosing and stoppering machine, are responsible for batch non-uniformity, as they influence respectively the drying time and the flow resistance of single vials.

2. Study of the effect of the various causes of batch heterogeneity on product dynamics

The aim of this section is to investigate the effect of some of the various causes that can affect the evolution of the product in a freeze-drying cycle, thus resulting in a non-homogeneous batch. Let us consider various vials placed in different positions in the drying chamber, and with differences in shelf temperature due to fluid circulation (see Figure 6), and let us compare the maximum product temperature during primary drying and the time required to complete primary drying. Results are summarized in Table 1.

In order to asses the effect of radiation from chamber walls it is possible to compare vials A and B: both vials are placed on the bottom tray, where pressure gradients along the shelf are small and, thus, the effect of fluid dynamics on the system is negligible, but while vial A is placed in the central part of the tray, where radiation has no effect (there is only a small radiation flux from the upper tray), vial B is placed in the external part of the tray, in front of the wall of the chamber, without any shield. It is worthwhile noticing that in the non-shielded vial the time required to complete the primary drying is significantly lower (about 17 %) and the interface temperature, that should be tightly controlled, may be 1° C higher. In any case, radiation from the side-walls affects the dynamics of a very low number of vials (only 6-7% of the vials of a batch in an industrial apparatus are affected by radiation as they are placed at the side of the tray) while in a small-scale apparatus, used for research and development purposes, the effect may be more important, and, thus, it is essential that the vials are shielded in order to obtain results that can be reliably scaled up.

To asses the effect of a non-uniform shelf temperature it is possible to compare results obtained for vials A and C: both are placed in the central part of the shelf, where radiation effects are negligible, but a shelf temperature higher of 3°C has been considered to study the dynamics of the product in vial C: the result is a reduction of the drying time of about 10%, and a maximum product temperature higher than that of vial A. This suggests the need for a tight control of shelf temperature during the process, also because it affects the dynamics of the whole batch. An example of the temperature and interface position evolution is shown in Figure 7 (l.h.s.).

In order to asses the effect of water vapor fluid dynamics it is possible to compare product evolution in vials A and D: while the first vial is placed in the point where the pressure is higher, the second one is placed at the border of the tray near the duct, where the pressure is lower. Radiation is neglected (i.e. vial D is supposed to be shielded), and the shelf temperature is assumed to be uniform on both trays in order to point out only the effect of the

fluid dynamics on the system. It is possible to see from Table 1 that chamber pressure gradients have a small influence on the time required to complete primary drying, while they may be responsible for a difference in the product temperature up to 0.5 °C for the case considered.

It must be highlighted that while radiation effect can be reduced by proper vials shielding, and the effect of a non-uniform shelf temperature can be minimized up to a certain extent, the effect of water vapor fluid dynamics, that is much more relevant in large-scale units, while it is almost negligible in small-scale apparatus, can be reduced only if the design of the apparatus is revised, i.e. if one or more geometrical parameters that affect the pressure gradients in the chamber are modified (i.e. the distance between the shelves or the duct position).

Finally, when the leakage control is used to vary the chamber pressure, the presence of the inert and its distribution in the drying chamber can be another source of heterogeneity among the various vials. Beside leakage control, inert gases enter anyway the chamber through normal chamber leakage and, mainly, as gases previously absorbed in the liquid. The latter case is not responsible for batch heterogeneity, but it can affect the freeze-drying process. Even if it has been shown that in certain situations the inert can form segregated zones in a marginal part of the chamber, depending on the geometry and operating conditions, the inert fraction in the chamber can vary between 0 and 40% (these are the minimum and maximum values that are usually found in standard equipment). It is very difficult to estimate the composition of the atmosphere around a vial that affects the evolution of the product and, thus, the behavior of a vial in two limit situations has been investigated and is shown in Figure 7 (r.h.s.). In this example the total pressure is 10 Pa, but for some vials this corresponds to only 6 Pa of water partial pressure due to the presence of the inert. This affects the equilibrium temperature and, thus, the product temperature, as well as the driving force for the mass transfer, thus resulting in a different drying time. This effect can be enhanced by the particular fluid dynamics of the inert in the drying chamber. To this purpose, a two-scale model, that couples the dynamics of the product in each vial with the fluid dynamics of the water vapor and of the inert gas in the chamber, could be usefully employed for such investigations (Barresi et al., 2008; Rasetto, 2009).

3. Development of a modified DPE algorithm for heterogeneous batches

As stated in the Introduction, monitoring and controlling the primary drying by means of non-invasive sensors, able to estimate those parameters not directly measurable (sublimating

interface temperature and position, heat and mass transfer coefficients), is important to guarantee the final quality of the product. The *Dynamic Parameters Estimation* (DPE) algorithm (Velardi and Barresi, 2008b; Velardi et al., 2008), is an advanced model-based monitoring tool that can be used to achieve this result.

During the Pressure Rise Test (PRT) the dynamics of the pressure in the chamber of volume V_c is given by:

$$P_c = p_w + p_{in} = p_w + F_{leak}t + p_{in,0} \qquad \text{for } t \geq 0 \tag{3}$$

where F_{leak} is the leakage rate, and *w* and *in* refer to water and inert respectively. The contribution to the pressure variation in the chamber of the generic *j*-th vial of internal section *A* is given by:

$$\frac{dp_{w,j}}{dt} = \frac{1}{V_c}\frac{RT_c}{M_w}A\left(R_{s,j} + \frac{RT_{i,j}}{M_w}\frac{L_j - L_{f,j}}{k_{1,j}}\right)^{-1}\left(p_{w,i,j}\left(T_{i,j}\right) - p_{w,c}\right) \tag{4}$$

with adequate boundary and initial conditions. $k_{1,j}$ is the diffusivity of water vapor in the dried layer, $R_{s,j}$ is the stopper resistance to vapor flow, $T_{i,j}$ is the temperature of the sublimation interface, and L_j is the product thickness, while $L_{f,j}$ is the thickness of the frozen layer. In the general case, as discussed before, also the initial product thickness and the stopper resistance (dependent on stopper positioning) can be variable from vial to vial. For sake of simplicity, only the variability of the frozen layer thickness, interface temperature, and vapor effective diffusivity, dependent on the structure of the dried layer generated by the nucleation step, will be considered in the following, neglecting the resistance of the stopper, thus eq. (4) becomes:

$$\frac{dp_{w,j}}{dt} = \frac{1}{V_c}A\frac{T_c}{T_{i,j}}\frac{k_{1,j}}{L_j - L_{f,j}}\left(p_{w,i,j}\left(T_{i,j}\right) - p_{w,c}\right) \tag{5}$$

where $\left(L_j - L_{f,j}\right)/k_{1,j}$ explicitates the resistance to mass transfer of the cake (R_P) in terms of dried product thickness and vapor diffusivity. In case of homogeneous batch eq. (5) holds for all the N_v vials and, assuming that $T_c = T_i$, we obtain:

$$\frac{dp_w}{dt} = \sum_{j=1}^{N_v}\frac{dp_{w,j}}{dt} = N_v\frac{1}{V_c}A\frac{k_1}{L - L_f}\left(p_i\left(T_i\right) - p_{w,c}\right) \tag{6}$$

The values of L_f, T_i and k_1 (the subscript "*j*" has been deleted as the values are assumed to be equal in all the vials) are thus calculated in order to have a best fit between the calculated values of chamber pressure and the measured data: the Levenberg-Marquardt method is used to minimize a cost function given by the difference between the calculated values of the chamber pressure and the values measured during the PRT.

Actually, vials placed in different positions have different behaviors because of the

various causes previously described. Depending on the apparatus scale (small or industrial scale) the contribution of the fluid dynamics, or of the radiation, on the product unevenness is different, but in both cases they affect the DPE results because the pressure rise contribution of the single vials is not the same, but it depends on the position of the vial. This aspect can be particularly relevant near the end point of primary drying, when some vials have already completed the drying and, thus, they do not contribute to the pressure rise measured. Thus, eq. (6) is written as:

$$\frac{dp_w}{dt} = \sum_{j=1}^{N_v^*} \frac{dp_{w,j}}{dt} = \sum_{j=1}^{N_v^*} \left[\frac{1}{V_c} \frac{T_c}{T_{i,j}} A \frac{k_{1,j}}{L_j - L_{f,j}} \left(p_{w,i,j}\left(T_{i,j}\right) - p_{w,c} \right) \right] \tag{7}$$

where N_v^* is the number of vials where primary drying is not yet terminated. Velardi et al. (2008) simplified eq. (7) by introducing a correction coefficient γ which accounts for the heterogeneity of the batch, whose expression is given by:

$$\gamma = \frac{\sum_{j=1}^{N_v^*} \left[\frac{k_{1,j}}{T_{i,j}} \frac{p_{w,i,j}\left(T_{i,j}\right) - p_{w,c}}{L - L_{f,j}} \right]}{N_v \frac{k_1}{T_i} \left(\frac{p_{w,i}\left(T_i\right) - p_{w,c}}{L - L_f} \right)} \tag{8}$$

where L_f, T_i and k_1 are the average values of the various parameters. Substituting the expression of γ in eq. (7), we obtain:

$$\frac{dp_w}{dt} = \gamma N_v A \frac{k_1}{L - L_f} \left(p_{w,i}\left(T_i\right) - p_{w,c} \right) \tag{9}$$

which is similar, a part from the parameter γ, to eq. (6), used for the case of homogeneous batch.

Considering that the parameters L_f, T_i and k_1 are distributed around a mean value with a certain variance, it is possible to expand in series of powers the r.h.s. of eq. (7) around the mean values of the various parameters, thus obtaining:

$$\frac{dp_w}{dt} = N_v A k_1 \left(\frac{p_{w,i}\left(T_i\right) - p_{w,c}}{L - L_f} \right) \left(1 + f\right) \tag{10}$$

where L_f, T_i and k_1 are the mean values of the various parameters and f is a complex non-linear function of the variance (and of the covariances) of the parameters. Details are given in the Appendix. It is possible to relate the γ parameter to the variance and covariance of the previous parameters, showing that:

$$\gamma = 1 + f\left(\sigma_{T_i}, \sigma_{L_d}, \sigma_{T_i,L_d}, \sigma_{T_i,L_d}, \sigma_{k_1,L_d}, \sigma_{T_i,k_1}\right) \tag{11}$$

or the γ parameter could be estimated together with the other parameters by the best fitting of the experimental data, even if the strong correlation between this parameter and k_1 make difficult to obtain reliable values. In any case it could be evaluated independently by using sensors that monitor single vials.

4. DPE in case of radiation

The experimental campaign undertaken to investigate the effects of radiation into the drying chamber gives also some information about how the results of DPE are affected in case of different radiating contributions. As stated above, during the primary drying the side-wall radiation affects the heat flux to the vials placed at the borders of the trays: as a consequence, the temperature profile is modified and the sublimation flux is higher. Thus, near the end of primary drying the number of sublimating vials can be progressively reduced.

If the radiating heat flux is limited, it can be accounted for by considering an effective heat transfer coefficient and, if all the vials are in the same conditions, as it may happen with a small lot in a small apparatus where all the vials are radiated, DPE can still be used, even if with caution (Barresi et al., 2009).

If the fraction of the vials affected by radiation is small, as in large-scale equipment with a large number of vials, the value obtained is representative of almost the whole batch, even if a certain number of vial has significantly higher drying rate and temperature. Figure 8 (l.h.s.) compares a curve of pressure rise obtained for a large scale apparatus with the curve that would be obtained assuming all the vials shielded and with that obtained assuming all the vials radiated: the values of the parameters that can be obtained from the PRT are thus representative of the largest part of the vials which are shielded. The situation in the small-scale apparatus is quite different, as it is evidenced by Figure 8 (r.h.s.). In this case radiation effects are more important as the contribution of the vials positioned on the side of the plate to the PRT curve is significant.

Beside that, it has been also studied the effect of the radiation heat flux coming from the upper heating shelf. In this case no heterogeneity is induced into the batch, but if its flux is high, DPE is not able to predict anymore the product temperature, as it is shown in Figure 9. In fact, in this case the product temperature profile is reversed, i.e. the interface temperature is higher than that at the vial bottom, due to heat accumulation into the dried layer. Thus, in case of high radiation from above, the mathematical model of DPE algorithm should be modified, including also the enthalpy balance of the dried layer.

5. The control system

In this section a model-based controller, named *LyoDriver* (LD), is presented. This novel control tool is able to lead primary drying toward target product specifications exploiting outcomes given by DPE, and can be adopted both for scouting, that is to find the near-optimal "recipe" in a single run, and in production, to guarantee that the constraints given for the product are respected, notwithstanding disturbances and changes in operating conditions. In fact, *LyoDriver* continuously adjusts the shelf temperature in such a way that product temperature never overcomes its target, even if it is very close to it, and never impairs product integrity; on the other hand, as the product temperature is maintained close to its upper bound, this control system minimizes the drying time through an optimal heating strategy. A crucial point to be stressed is that *LyoDriver* takes also into account the actual thermal dynamics of the freeze-dryer and, furthermore, the temperature rise due to the PRT and the control overshoots. Details about the algorithm can be found in Barresi et al. (2009), Pisano (2009), and Pisano et al. (2009).

Figure 10 shows an example of application of LD to control a freeze-drying cycle. The freezing phase was run at 223 K and, then, the heating fluid temperature was automatically manipulated by LD controller taking into account that T_{MAX} was set at 241.15 K, corresponding to the glass transition temperature measured by DSC. It can be evidenced that the product temperature is maintained close to the maximum allowed value, thus maximizing the sublimation rate, and that this value is not overcome. By this way, the cycle is shortened, without risk for the product, because, though at the beginning the heating up is set at the maximum value allowed, the evolution of the temperature of the product is predicted, and the occurrence of temperature overshoot due to control actions is avoided. In this case the heat transfer from the shelf controls the sublimation rate and the fluid temperature is set at about -7°C in the second part of the primary drying step: this value, significantly higher than the product temperature, is the one that ensures maximum sublimation rate, while pressure set-point is not very influent. In some cases the manipulation of the fluid temperature can be not sufficient to have a complete control of the process: when the resistance to mass transfer is much more important, or rather the vapor transport trough the dried layer controls the drying rate, LD controller is not able anymore to optimize the process rate by manipulating only the shelf temperature (Galan et al., 2007). Thus, in this case a reduction of chamber pressure is convenient to increase the sublimation rate and decrease product temperature (Barresi et al., 2009; Fissore et al., 2009).

Finally, another point to be stressed is that LD bases its calculations on DPE outcomes,

that supplies an average estimation of the system state. These estimations are generally representative of the large part of batch vials, at least in case of moderate unevenness, but toward the end of primary drying non-uniformity can significantly affect the DPE outcomes, as evidenced in Figure 10: in fact, the apparent decrease of the estimated product temperature observed after 12 h can be partly due to ill-conditioning of the numerical problem, but is certainly strongly related with the fact that some vials have completed sublimation. Anyway, according to the targets indicated by the US Foods and Drugs Administration, an optimal process control should take also into account the batch unevenness, applying an optimal heating strategy so that the final product quality of the entire batch, including the edge-vials, is guaranteed. To this purpose, there are two possible control approaches. The former consists in monitoring in-line not only the average state of the batch, but also that of the edge vials characterized by an higher product temperature, choosing the best heating strategy according to their state. An advanced DPE algorithm would be requested to monitor radiated vial; in particular, the DPE algorithm should be modified in such a way that it is able to interpret the pressure rise curve simulating the batch not as a whole, but as the sum of several vial types (both vials placed in the core and on the side of the batch). The latter involves a 2-scales model of a freeze-drying process (Barresi et al., 2008; Rasetto, 2009), or rather a tool that couples the results of the fluid dynamics of the water vapor inside the drying chamber obtained through CFD simulations, and a detailed one-dimensional model of the drying that takes also into account radiation from the chamber side-wall. By this way, it is possible to track the dynamics of vials placed in different positions of the batch and, thus, to estimate the batch variance for certain operating conditions. Then, this information could be used to set the tuning parameters of the controller in such a way that it chooses the best control strategy to meet the product specifications in all the vials. As an alternative, the DPE algorithm can be coupled with a system that estimates the variance of the batch using sensors that monitor the single vials, and the control system can calculate the control actions on the basis of the mean product temperature and of the temperature of the radiated vials.

Conclusions

Since during the primary drying product damages (e.g. product collapse) can occur, monitoring and controlling of this phase is very important to guarantee the desired final product quality: in particular, product temperature has to be maintained below the collapse (or

melting) value during the cycle. To this purpose the development of model-based monitoring tools is encouraged.

The attainment of the goal is made more difficult to get by the fact that the vials do not undergo the same freeze-drying history, not only because of the well known radiation effect, or because the shelf temperature is not uniform, but also because of the flow field inside the freeze-dryer chamber. Moreover, while in small-scale units, used for recipe development, radiation from chamber walls plays an important role, in the industrial-scale apparatus the role of pressure gradients is much more important: this has to be taken into account during process scale-up.

The effect of batch heterogeneity on the performance of the monitoring tools based on the PRT, and on that of the control system, has been discussed and, finally, a control tool, *LyoDriver*, has been presented and shown to be effective to control and to optimize a freeze-drying cycle. Moreover, it can be exploited to determine with few tests the optimal recipe for the primary drying of the product of interest, or rather the optimal heating policy for a given value of chamber pressure.

Acknowledgements

This work was partially supported by Telstar-Industrial (Terrassa, Spain).

List of symbols

A	internal cross surface section of the vial, m^2
A_v	bottom surface of the vial, m^2
d_v	vial internal diameter, mm
F_{leak}	leakage rate, Pa s^{-1}
f	parameter that is a function of the variance of the batch
ΔH_s	enthalpy of sublimation, J kg^{-1}
K_v	heat transfer coefficient, J $m^{-2}s^{-1}K^{-1}$
k_1	effective diffusivity of water vapor in the dried layer, m^2s^{-1}
L	total product thickness, m
L_d	dried layer thickness, m

L_f	frozen layer thickness, m
M_w	molecular weight of water, kg kmol^{-1}
m	mass of ice, kg
N_v	number of vials
N_v^*	number of vials still sublimating
p	partial pressure, Pa
R	ideal gas constant, J kmol^{-1}K^{-1}
R_P	mass transfer resistance in the dried layer $= \frac{L - L_f}{k_1} \frac{RT_i}{M_w}$, m s^{-1}
R_S	mass transfer resistance in the stopper, m s^{-1}
t	time, s
T	temperature, K
T_c	temperature in the drying chamber, K
T_{MAX}	maximum temperature allowed by the product, K
V_c	chamber volume, m^3
x, y	coordinates identifying the position of a vial on a tray, m
z	axial position, m

Greeks

γ	correction coefficient
σ	variance

Subscripts

0	value at time $t = 0$
B	value at the bottom of the vial
c	chamber
i	interface
in	inert
shelf	heating shelf
w	water vapor

Abbreviations

CFD	Computational Fluid Dynamics

DPE	*Dynamic Parameters Estimation*
LD	*LyoDriver*
MTM	Manometric Temperature Measurement
PRT	Pressure Rise Test

References

Barresi, A. A., Rasetto, V., Pisano, R., Fissore, D., Marchisio, D. L., Vanni, M. (2008). Multiscale modelling of freeze-drying for optimisation and quality control of pharmaceutical products. Proceedings of 5th Chemical Engineering Conference for Collaborative Research in Eastern Mediterranean Countries EMCC5, Cetraro (CS), Italy, 24-29 May, 390-393.

Barresi, A. A., Pisano, R., Fissore, D., Rasetto, V., Velardi, S. A., Vallan, A., Parvis, M., Galan, M. (2009). Monitoring of the primary drying of a lyophilization process in vials. Chemical Engineering and Processing, 48, 403-423.

Ferziger, J. H., Peric, M. (2002). *Computational Methods for Fluid Dynamics*. Springer: Berlin.

Fissore, D., Velardi, S. A., Barresi A. A. (2008). In-line control of a freeze-drying process in vial. Drying Technology, 26, 685-694.

Fissore D., Pisano R., Barresi A. A. (2009). On the design of an in-line control system for a vial freeze-drying process: the role of chamber pressure. Chemical Product and Process Modeling (special issue on Process modeling & control, D. Manca and R. Aguilar-López Eds.),), 4(2), Article 9, 22 pp.

Galan, M., Velardi, S. A., Pisano, R., Rasetto, V., Barresi A. A. (2007). A gentle PAT approach to in-line control of the lyophilization process. Refrigeration Science and Technology Proceedings No 2007-3, "New ventures in Freeze-Drying", Strasbourg, France, 7-9 November. CD-ROM Edition, Institut International du Froid, Paris, 17 pp.

Gan, K. H., Bruttini, R., Crosser, O. K., Liapis, A. A. (2004). Heating policies during the primary and secondary drying stages of the lyophilization process in vials: effects of the arrangement of vials in clusters of square and hexagonal arrays on trays. Drying Technology, 22, 1539-1575.

Gan, K. H., Bruttini, R., Crosser, O. K., Liapis, A. I. (2005a). Freeze-drying of pharmaceuticals in vials on trays: effects of drying chamber wall temperature and tray side on lyophilization performance. International Journal of Heat and Mass Transfer, 48, 1675-1687.

Gan, K. H., Crosser, O. K., Liapis, A. I., Bruttini, R. (2005b). Lyophilisation in vials on trays: effects of tray side. Drying Technology, 23, 341-363.

Gieseler, H., Kramer, T., Pikal, M. J. (2007). Use of Manometric Temperature Measurement (MTM) and SMART™ Freeze Dryer technology for development of an optimized

freeze-drying cycle. Journal of Pharmaceutical Sciences, 96, 3402–3418.

Kobayashi, M., Harashima, K., Sunama, R., Yao, A. R. (1991). Inter-vial variance of the sublimation rate in shelf freeze-dryer. Proceedings of 18th International Refrigeration Congress, Sainth Hyacinthe (Quebec), Canada, 1711-1715.

Liapis, A. I., Bruttini, R. (1995). Freeze-drying of pharmaceutical crystalline and amorphous solutes in vials: Dynamic multi-dimensional models of the primary and secondary drying stages and qualitative features of the moving interface. Drying Technology, 13, 43–72.

Liapis, A. I., Pikal, M. J., Bruttini, R. (1996). Research and development needs and opportunities in freeze drying. Drying Technology, 14, 1265–1300.

Milton, N., Pikal, M. J., Roy, M. L., Nail, S. L. (1997). Evaluation of manometric temperature measurement as a method of monitoring product temperature during lyophilisation. PDA Journal of Pharmaceuticals Science, 51, 7-16.

Oetjen, G. W. (1999). *Freeze-drying*. Wiley-VCH Verlag, Weinheim.

Oetjen, G. W., Haseley, P. (2004). *Freeze-drying* (2nd edition). Wiley-VCH Verlag, Weinheim.

Pikal, M. J., Tang, X., Nail, S. L. (2005). Automated process control using manometric temperature measurement. United States Patent US 6,971,187 B1.

Pisano, R. (2009). Monitoring and control of a freeze-drying process of pharmaceutical products in vials. PhD Dissertation, Politecnico di Torino, Italy.

Pisano R., Fissore D., Velardi S. A., Barresi A. A. (2009). In-line optimization and control of an industrial freeze-drying process for pharmaceuticals. Journal of Pharmaceutical Sciences. Submitted.

Rasetto, V., Pisano R., Barresi A. A., Vallan A. (2008a). Modelling and experimental investigation of radiation effects in a freeze-drying process. Proceedings of 5th Chemical Engineering Conference for Collaborative Research in Eastern Mediterranean Countries EMCC5, Cetraro (CS), Italy, 24-29 May, 394-397.

Rasetto, V., Marchisio, D. L., Fissore, D., Barresi, A. A. (2008b). Model-based monitoring of a non-uniform batch in a freeze-drying process. Proceedings of the 18th European Symposium on Computer Aided Process Engineering – ESCAPE 18 (B. Braunschweig and X. Joulia Eds.), Lyon, France, 1-4 June. Computer Aided Chemical Engineering Series, Vol. 24. Elsevier B.V./Ltd. [paper 210].

Rasetto, V. (2009). Use of mathematical models in the freeze-drying field: process understanding and optimal equipment design. PhD Dissertation, Politecnico di Torino,

Italy.

Sadikoglu, H., Liapis, A. I. (1997). Mathematical modelling of the primary and secondary drying stages of bulk solution freeze drying in trays: Parameter estimation and model discrimination by comparison of theoretical results with experimental data. Drying Technology, 15, 791–810.

Sadikoglu, H., Ozdemir, M., Seker, M. (2006). Freeze-drying of pharmaceutical products: Research and development needs. Drying Technology, 24, 849-861.

Sennhenn, B., Gehrmann, D., Firus, A. (2005). Freeze drying apparatus. United States Patent US 6,931,754 B2.

Tang, X., Pikal, M. J. (2004). Design of freeze-drying processes for pharmaceuticals: Practical advice. Pharmaceutical Research, 21, 191–200.

Tang X. C., Nail, S. L., Pikal, M. J. (2005). Freeze-drying process design by Manometric Temperature Measurement: design of a smart freeze-dryer. Pharmaceutical Research, 22, 685-700.

Tang, X. C., Nail, S. L., Pikal, M. J. (2006a). Evaluation of manometric temperature measurement, a Process Analytical Technology tool for freeze-drying, part II: measurement of dry-layer resistance. AAPS Pharmaceutical Science and Technology, 7, article 93, 9 pp. (http://www.aapspharmscitech.org).

Tang, X. C., Nail, S. L., Pikal, M. J. (2006b). Evaluation of manometric temperature measurement (MTM), a Process Analytical Technology tool in freeze drying, part III: heat and mass transfer measurement. AAPS Pharmaceutical Science and Technology, 7, article 97, 7 pp. (http://www.aapspharmscitech.org).

Velardi, S. A., Barresi, A. A. (2008a). Development of simplified models for the freeze-drying process and investigation of the optimal operating conditions. Chemical Engineering Research &. Design, 86, 9-22.

Velardi, S. A., Barresi, A. A. (2008b). Method and system for controlling a freeze drying process. International Publication No. WO/2008/034855 A2, World Intellectual Property Organization (International Application No. PCT/EP2007/059921).

Velardi, S. A., Rasetto, V., Barresi, A. A. (2008). Dynamic Parameters Estimation Method: advanced Manometric Temperature Measurement approach for freeze-drying monitoring of pharmaceutical, Industrial & Engineering Chemistry Research, 47, 8445-8457.

Appendix

Equation (7) describes the contribution of the various vials to the pressure rise. Let us assume that at the beginning of the test the various vials have values of k_1, L_f, and of T_i (and, thus, of $p_{w,i}$) distributed around a mean value and that this distribution remain constant. The r.h.s. of eq. (7) can thus be developed in series of powers around the mean values of the various parameters, i.e. $\overline{k}_1$, $\overline{L}_f$, $\overline{T}_i$, thus obtaining:

$$
\begin{aligned}
&\frac{V_c}{AT_c}\frac{dp_w}{dt} = N_v\frac{\overline{k}_1\overline{p}_i}{\overline{T}_i\overline{L}_d} + \sum_{j=1}^{N_v}\frac{\partial}{\partial T_{i,j}}\left(\frac{k_{1,j}p_{w,i,j}}{T_{i,j}L_{d,j}}\right)\Bigg|_{\overline{T}_i,\overline{k}_1,\overline{L}_d}\left(T_{i,j}-\overline{T}_i\right) + \sum_{j=1}^{N_v}\frac{\partial}{\partial L_{d,j}}\left(\frac{k_{1,j}p_{w,i,j}}{T_{i,j}L_{d,j}}\right)\Bigg|_{\overline{T}_i,\overline{k}_1,\overline{L}_d}\left(L_{d,j}-\overline{L}_d\right) + \\
&+\sum_{j=1}^{N_v}\frac{\partial}{\partial k_{1,j}}\left(\frac{k_{1,j}p_{w,i,j}}{T_{i,j}L_{d,j}}\right)\Bigg|_{\overline{T}_i,\overline{k}_1,\overline{L}_d}\left(k_{1,j}-\overline{k}_1\right) + \sum_{j=1}^{N_v}\frac{\partial^2}{\partial {T_{i,j}}^2}\left(\frac{k_{1,j}p_{w,i,j}}{T_{i,j}L_{d,j}}\right)\Bigg|_{\overline{T}_i,\overline{k}_1,\overline{L}_d}\left(T_{i,j}-\overline{T}_i\right)^2 + \\
&+\sum_{j=1}^{N_v}\frac{\partial^2}{\partial {L_{d,j}}^2}\left(\frac{k_{1,j}p_{w,i,j}}{T_{i,j}L_{d,j}}\right)\Bigg|_{\overline{T}_i,\overline{k}_1,\overline{L}_d}\left(L_{d,j}-\overline{L}_d\right)^2 + \sum_{j=1}^{N_v}\frac{\partial^2}{\partial {k_{1,j}}^2}\left(\frac{k_{1,j}p_{w,i,j}}{T_{i,j}L_{d,j}}\right)\Bigg|_{\overline{T}_i,\overline{k}_1,\overline{L}_d}\left(k_{1,j}-\overline{k}_1\right)^2 + \\
&+\sum_{j=1}^{N_v}\frac{\partial}{\partial T_{i,j}}\frac{\partial}{\partial L_{d,j}}\left(\frac{k_{1,j}p_{w,i,j}}{T_{i,j}L_{d,j}}\right)\Bigg|_{\overline{T}_i,\overline{k}_1,\overline{L}_d}\left(T_{i,j}-\overline{T}_i\right)\left(L_{d,j}-\overline{L}_d\right) + \\
&+\sum_{j=1}^{N_v}\frac{\partial}{\partial L_{d,j}}\frac{\partial}{\partial k_{1,j}}\left(\frac{k_{1,j}p_{w,i,j}}{T_{i,j}L_{d,j}}\right)\Bigg|_{\overline{T}_i,\overline{k}_1,\overline{L}_d}\left(L_{d,j}-\overline{L}_d\right)\left(k_{1,j}-\overline{k}_1\right) + \\
&+\sum_{j=1}^{N_v}\frac{\partial}{\partial T_{i,j}}\frac{\partial}{\partial k_{1,j}}\left(\frac{k_{1,j}p_{w,i,j}}{T_{i,j}L_{d,j}}\right)\Bigg|_{\overline{T}_i,\overline{k}_1,\overline{L}_d}\left(T_{i,j}-\overline{T}_i\right)\left(k_{1,j}-\overline{k}_1\right) + \\
&-N_v p_{w,c}\frac{\overline{k}_1}{\overline{T}_i\overline{L}_d} - p_{w,c}\sum_{j=1}^{N_v}\frac{\partial}{\partial T_{i,j}}\left(\frac{\overline{k}_1}{\overline{T}_i\overline{L}_d}\right)\Bigg|_{\overline{T}_i,\overline{k}_1,\overline{L}_d}\left(T_{i,j}-\overline{T}_i\right) - p_{w,c}\sum_{j=1}^{N_v}\frac{\partial}{\partial L_{d,j}}\left(\frac{\overline{k}_1}{\overline{T}_i\overline{L}_d}\right)\Bigg|_{\overline{T}_i,\overline{k}_1,\overline{L}_d}\left(L_{d,j}-\overline{L}_d\right) + \\
&-p_{w,c}\sum_{j=1}^{N_v}\frac{\partial}{\partial k_{1,j}}\left(\frac{\overline{k}_1}{\overline{T}_i\overline{L}_d}\right)\Bigg|_{\overline{T}_i,\overline{k}_1,\overline{L}_d}\left(k_{1,j}-\overline{k}_1\right) - p_{w,c}\sum_{j=1}^{N_v}\frac{\partial^2}{\partial {T_{i,j}}^2}\left(\frac{\overline{k}_1}{\overline{T}_i\overline{L}_d}\right)\Bigg|_{\overline{T}_i,\overline{k}_1,\overline{L}_d}\left(T_{i,j}-\overline{T}_i\right)^2 + \\
&-p_{w,c}\sum_{j=1}^{N_v}\frac{\partial^2}{\partial {L_{d,j}}^2}\left(\frac{\overline{k}_1}{\overline{T}_i\overline{L}_d}\right)\Bigg|_{\overline{T}_i,\overline{k}_1,\overline{L}_d}\left(L_{d,j}-\overline{L}_d\right)^2 - p_{w,c}\sum_{j=1}^{N_v}\frac{\partial^2}{\partial {k_{1,j}}^2}\left(\frac{\overline{k}_1}{\overline{T}_i\overline{L}_d}\right)\Bigg|_{\overline{T}_i,\overline{k}_1,\overline{L}_d}\left(k_{1,j}-\overline{k}_1\right)^2 + \\
&-p_{w,c}\sum_{j=1}^{N_v}\frac{\partial}{\partial T_{i,j}}\frac{\partial}{\partial L_{d,j}}\left(\frac{\overline{k}_1}{\overline{T}_i\overline{L}_d}\right)\Bigg|_{\overline{T}_i,\overline{k}_1,\overline{L}_d}\left(T_{i,j}-\overline{T}_i\right)\left(L_{d,j}-\overline{L}_d\right) + \\
&-p_{w,c}\sum_{j=1}^{N_v}\frac{\partial}{\partial L_{d,j}}\frac{\partial}{\partial k_{1,j}}\left(\frac{\overline{k}_1}{\overline{T}_i\overline{L}_d}\right)\Bigg|_{\overline{T}_i,\overline{k}_1,\overline{L}_d}\left(L_{d,j}-\overline{L}_d\right)\left(k_{1,j}-\overline{k}_1\right) + \\
&-p_{w,c}\sum_{j=1}^{N_v}\frac{\partial}{\partial T_{i,j}}\frac{\partial}{\partial k_{1,j}}\left(\frac{\overline{k}_1}{\overline{T}_i\overline{L}_d}\right)\Bigg|_{\overline{T}_i,\overline{k}_1,\overline{L}_d}\left(T_{i,j}-\overline{T}_i\right)\left(k_{1,j}-\overline{k}_1\right)
\end{aligned}
\tag{A.1}
$$

After the calculation of the various derivatives in eq. (A.1) we obtain:

$$\frac{V_c}{AT_c}\frac{dp_w}{dt} = N_v \frac{\bar{k}_1 \bar{p}_i}{\bar{T}_i \bar{L}_d} - \frac{\bar{k}_1 \bar{p}_i}{\bar{T}_i \bar{L}_d}\sum_{j=1}^{N_v}\frac{\left(T_{i,j}-\bar{T}_i\right)}{\bar{T}_i} + \frac{\bar{k}_1}{\bar{T}_i \bar{L}_d}\sum_{j=1}^{N_v}\left(\frac{\partial p_{w,i,j}}{\partial T_{i,j}}\right)\Bigg|_{\bar{T}_i,\bar{k}_1,\bar{L}_d}\left(T_{i,j}-\bar{T}_i\right) +$$

$$-\frac{\bar{k}_1 \bar{p}_i}{\bar{L}_d \bar{T}_i}\sum_{j=1}^{N_v}\frac{\left(L_{d,j}-\bar{L}_d\right)}{\bar{L}_d} + \frac{\bar{p}_i}{\bar{T}_i \bar{L}_d}\sum_{j=1}^{N_v}\left(k_{1,j}-\bar{k}_1\right) +$$

$$+\frac{2\bar{k}_1 \bar{p}_i}{\bar{T}_i \bar{L}_d}\sum_{j=1}^{N_v}\frac{\left(T_{i,j}-\bar{T}_i\right)^2}{\bar{T}_i^2} - 2\frac{\bar{k}_1}{\bar{L}_d}\sum_{j=1}^{N_v}\left(\frac{\partial p_{w,i,j}}{\partial T_{i,j}}\right)\Bigg|_{\bar{T}_i,\bar{k}_1,\bar{L}_d}\frac{\left(T_{i,j}-\bar{T}_i\right)^2}{\bar{T}_i^2} +$$

$$+\frac{\bar{k}_1}{\bar{T}_i \bar{L}_d}\sum_{j=1}^{N_v}\left(\frac{\partial^2 p_{w,i,j}}{\partial {T_{i,j}}^2}\right)\Bigg|_{\bar{T}_i,\bar{k}_1,\bar{L}_d}\left(T_{i,j}-\bar{T}_i\right)^2 + 2\left(\frac{\bar{k}_1 \bar{p}_i}{\bar{L}_d \bar{T}_i}\right)\sum_{j=1}^{N_v}\frac{\left(L_{d,j}-\bar{L}_d\right)^2}{{\bar{L}_d}^2} +$$

$$+\frac{\bar{k}_1 \bar{p}_i}{\bar{L}_d \bar{T}_i}\sum_{j=1}^{N_v}\frac{\left(T_{i,j}-\bar{T}_i\right)}{\bar{T}_i}\frac{\left(L_{d,j}-\bar{L}_d\right)}{\bar{L}_d} - \frac{\bar{k}_1}{\bar{L}_d}\sum_{j=1}^{N_v}\left(\frac{\partial p_{w,i,j}}{\partial T_{i,j}}\right)\Bigg|_{\bar{T}_i,\bar{k}_1,\bar{L}_d}\frac{\left(T_{i,j}-\bar{T}_i\right)}{\bar{T}_i}\frac{\left(L_{d,j}-\bar{L}_d\right)}{\bar{L}_d} +$$

$$-\left(\frac{\bar{p}_i}{\bar{L}_d \bar{T}_i}\right)\sum_{j=1}^{N_v}\frac{\left(L_{d,j}-\bar{L}_d\right)\left(k_{1,j}-\bar{k}_1\right)}{\bar{L}_d} - \frac{\bar{p}_i}{\bar{L}_d \bar{T}_i}\sum_{j=1}^{N_v}\frac{\left(T_{i,j}-\bar{T}_i\right)}{\bar{T}_i}\left(k_{1,j}-\bar{k}_1\right) +$$

$$+\frac{1}{\bar{L}_d}\sum_{j=1}^{N_v}\left(\frac{\partial p_{w,i,j}}{\partial T_{i,j}}\right)\Bigg|_{\bar{T}_i,\bar{k}_1,\bar{L}_d}\frac{\left(T_{i,j}-\bar{T}_i\right)}{\bar{T}_i}\left(k_{1,j}-\bar{k}_1\right) +$$

$$-N_v p_{w,c}\frac{\bar{k}_1}{\bar{T}_i \bar{L}_d} + p_{w,c}\frac{\bar{k}_1}{\bar{T}_i \bar{L}_d}\sum_{j=1}^{N_v}\frac{\left(T_{i,j}-\bar{T}_i\right)}{\bar{T}_i} + p_{w,c}\sum_{j=1}^{N_v}\frac{\bar{k}_1}{\bar{T}_i \bar{L}_d}\frac{\left(L_{d,j}-\bar{L}_d\right)}{\bar{L}_d} - p_{w,c}\frac{1}{\bar{T}_i \bar{L}_d}\sum_{j=1}^{N_v}\left(k_{1,j}-\bar{k}_1\right) +$$

$$-p_{w,c}\frac{2\bar{k}_1}{\bar{T}_i \bar{L}_d}\sum_{j=1}^{N_v}\frac{\left(T_{i,j}-\bar{T}_i\right)^2}{\bar{T}_i^2} - p_{w,c}\frac{2\bar{k}_1}{\bar{T}_i \bar{L}_d}\sum_{j=1}^{N_v}\frac{\left(L_{d,j}-\bar{L}_d\right)^2}{{\bar{L}_d}^2} + \tag{A.2}$$

$$-p_{w,c}\frac{\bar{k}_1}{\bar{T}_i \bar{L}_d}\sum_{j=1}^{N_v}\frac{\left(T_{i,j}-\bar{T}_i\right)}{\bar{T}_i}\frac{\left(L_{d,j}-\bar{L}_d\right)}{\bar{L}_d} + p_{w,c}\frac{1}{\bar{T}_i \bar{L}_d}\sum_{j=1}^{N_v}\frac{\left(L_{d,j}-\bar{L}_d\right)}{\bar{L}_d}\left(k_{1,j}-\bar{k}_1\right) +$$

$$+p_{w,c}\frac{1}{\bar{T}_i \bar{L}_d}\sum_{j=1}^{N_v}\frac{\left(T_{i,j}-\bar{T}_i\right)}{\bar{T}_i}\left(k_{1,j}-\bar{k}_1\right)$$

Equation (A.2) can be simplified in:

$$\frac{V_c}{AT_c}\frac{dp_w}{dt} = N_v \frac{\bar{k}_1}{\bar{T}_i \bar{L}_d}\left(\bar{p}_i - p_{w,c}\right)\left[1 + f\left(\sigma_{T_i}, \sigma_{L_d}, \sigma_{T_i L_d}, \sigma_{k_1 L_d}, \sigma_{T_i k_1}\right)\right] \tag{A.3}$$

where:

$$f\left(\sigma_{T_i}, \sigma_{L_d}, \sigma_{T_i L_d}, \sigma_{k_1 L_d}, \sigma_{T_i k_1}\right) = \frac{\bar{p}_i}{\bar{p}_i - p_{w,c}} f_1\left(\sigma_{T_i}, \sigma_{L_d}, \sigma_{T_i L_d}, \sigma_{k_1 L_d}, \sigma_{T_i k_1}\right)] - \frac{p_{w,c}}{\bar{p}_i - p_{w,c}} f_2\left(\sigma_{T_i}, \sigma_{L_d}, \sigma_{T_i L_d}, \sigma_{k_1 L_d}, \sigma_{T_i k_1}\right) \tag{A.4}$$

$$f\left(\sigma_{T_i},\sigma_{L_d},\sigma_{T_iL_d},\sigma_{k_1L_d},\sigma_{T_ik_1}\right)=\frac{\overline{p}_i}{\overline{p}_i-p_{w,c}}f_1\left(\sigma_{T_i},\sigma_{L_d},\sigma_{T_iL_d},\sigma_{k_1L_d},\sigma_{T_ik_1}\right)+ -\frac{p_{w,c}}{\overline{p}_i-p_{w,c}}f_2\left(\sigma_{T_i},\sigma_{L_d},\sigma_{T_iL_d},\sigma_{k_1L_d},\sigma_{T_ik_1}\right) \tag{A.5}$$

$$f_1\left(\sigma_{T_i},\sigma_{L_d},\sigma_{T_iL_d},\sigma_{k_1L_d},\sigma_{T_ik_1}\right)=\sigma_{T_i}-2\sigma_{T_i}\frac{\overline{T}_i}{\overline{p}_i}\left(\frac{\partial p_{w,i,j}}{\partial T_{i,j}}\right)\Bigg|_{\overline{T}_i,\overline{k}_1,\overline{L}_d}+ +\sigma_{T_i}\frac{\overline{T}_i^2}{\overline{p}_i}\left(\frac{\partial^2 p_{w,i,j}}{\partial T_{i,j}^{\ 2}}\right)\Bigg|_{\overline{T}_i,\overline{k}_1,\overline{L}_d}+2\sigma_{L_d}-\frac{\overline{T}_i}{\overline{p}_i}\left(\frac{\partial p_{w,i,j}}{\partial T_{i,j}}\right)\Bigg|_{\overline{T}_i,\overline{k}_1,\overline{L}_d}\sigma_{T_iL_d}+ -\sigma_{k_1L_d}+\frac{\overline{T}_i}{\overline{p}_i}\left(\frac{\partial p_{w,i,j}}{\partial T_{i,j}}\right)\Bigg|_{\overline{T}_i,\overline{k}_1,\overline{L}_d}\sigma_{T_ik_1} \tag{A.6}$$

$$f_2\left(\sigma_{T_i},\sigma_{L_d},\sigma_{T_iL_d},\sigma_{k_1L_d},\sigma_{T_ik_1}\right)=2\sigma_{T_i}+2\sigma_{L_d}+\sigma_{T_iL_d}-\sigma_{k_1L_d}-\sigma_{T_ik_1} \tag{A.7}$$

Thus, by comparing eq. (A.3) with eq. (9) it is possible to get eq. (11).

List of Tables

List of Figures

drying in case of a vial placed in the centre of the batch (solid line) and at the edge of the shelf (dashed line). The operating conditions are the same of the data of Figure 1.

Figure 3 L.H.S. Pressure profiles over some plates in a large-scale apparatus with 17 (case A) and with 14 (case B) shelves (plus the top one), along the mean position on the shelf; the numbers identify the tray, starting from the bottom. The operating pressure set in the CFD code is 10 Pa and the mass flux is 1 kg $m^{-2}h^{-1}$.
R.H.S. Pressure profiles over some plates in a large-scale apparatus (16 shelves, plus the top one) along the mean *y*-position; shelf 1 (bottom): circle; shelf 12: square; shelf 16 (top): triangle. Values obtained at different mass flux: 1 kg $m^{-2}h^{-1}$ (case ϕ_1), 0.7 kg $m^{-2}h^{-1}$ (case ϕ_2) and 0.5 kg $m^{-2}h^{-1}$ (case ϕ_3);

Figure 4 Top: global 3D representation of pressure contour plots computed for all the plates (A), for the shelf at the bottom of the chamber (B) and for the shelf close to the duct (C) in the small scale apparatus .
Bottom: global 3D representation of pressure contour plots computed for all the plates (D), for the shelf at the bottom of the chamber (E) and for the shelf close to the duct (F) in the large scale apparatus.
The clearance between the plates is 100 mm, the operating pressure set in the CFD code is 10 Pa and the mass flux is 1 kg $m^{-2}h^{-1}$ for both the small and the large scale apparatus.

Figure 5 Inert mass fraction distribution in a small scale apparatus with the duct positioned at the bottom, with operating pressure in the CFD code set to 10 Pa. Sublimating vapor mass flux = 1 kg $m^{-2}h^{-1}$, inert mass flow equal to 12% of water flow. The inert is present only in the left part of the apparatus, close to the inlet.

Figure 6 Sketch of the large scale freeze-drier. The positions of some vials whose dynamics has been investigated to asses the effect of the various causes of heterogeneity is evidenced.

Figure 7 Comparison between the time evolution of the temperature (upper graph) and of the position of the sublimating interface (lower graph) in a freeze-drying cycle (P_c = 10 Pa, $d_v = 14 \cdot 10^{-3}$ m, $L = 7.2 \cdot 10^{-3}$ m).
l.h.s.: dynamics in vial placed over a shelf with T_{shelf} = -15°C (●) and in a vial placed over a shelf with T_{shelf} = -12°C (o).
r.h.s.: dynamics in a vial in case of pure water vapor (●) and in case of 40% of inert (o) in the local atmosphere (T_{shelf} = -15°C).

Figure 8 Estimated pressure evolution during a PRT in the large-scale (l.h.s.) and in the small scale (r.h.s.) freeze-dryer where radiation effects are taken into account (simbols). The curves resulting in case of uniform distribution corresponding to radiated vials (dashed line) and to shielded vials (solid line) are shown.

Figure 9 Product temperature evolution at the vial bottom detected by a thermocouple (solid line) and estimated by DPE (symbols) in case of the freeze-drying of a mannitol-dextran (6-14% by weight) solution (the freezing phase was run at 223 K, the primary drying at 303 K, P_c = 15 Pa, N_v = 99, d_v = 20.85 mm, L = 9.9 mm; time has been set equal to zero at the beginning of the primary drying).

Figure 10 Results obtained in a freeze-drying cycle of a 10% by weight sucrose solution using *LyoDriver* to monitor and control the primary drying stage: bottom product temperature estimated through DPE (symbols), the actual fluid temperature (——), its set-point calculated by *LyoDriver* controller (– – – –) and the limit temperature, T_{MAX} (- · - · - ·) are shown (P_c = 10 Pa, N_v = 175, d_v = 14.25, mm, $L = 7.2 \cdot 10^{-3}$ m).

Table 1

Case identifier	Shelf number	x, m	y, m	Radiation	T_{shelf}	Maximum product temperature, K	Drying time, h	Variation of maximum product temperature, K	Variation of drying time
A	1	1.03	0.440	NO	-15°C	239.7	11.9		
B	1	1.03	0.135	YES	-15°C	240.5	10.0	**0.8**	**-16.2%**
C	5	1.03	0.440	NO	-12°C	240.4	10.6	**0.7**	**-10.6%**
D	12	1.03	1.800	NO	-15°C	240.1	11.7	**0.5**	**-1.7%**

Figure 1

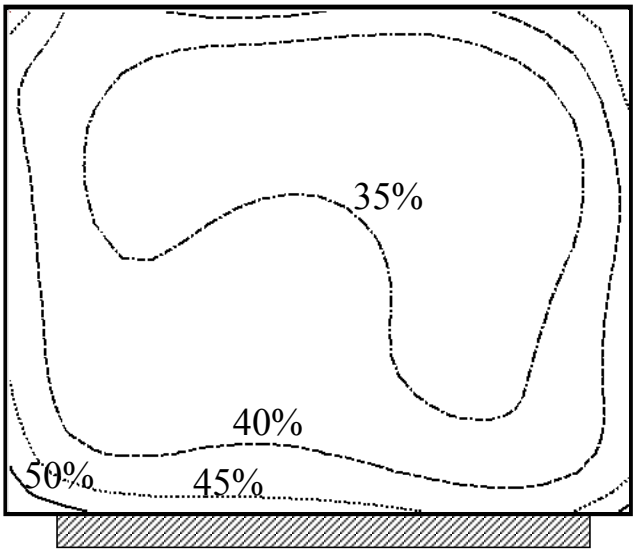

Figure 2

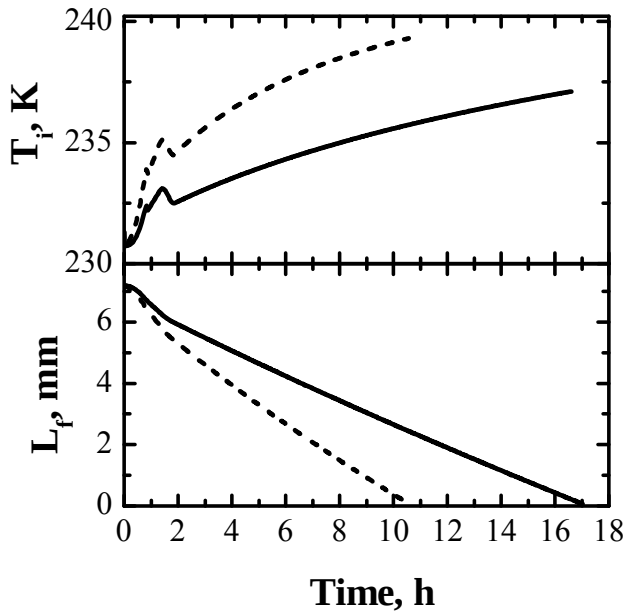

Figure 3

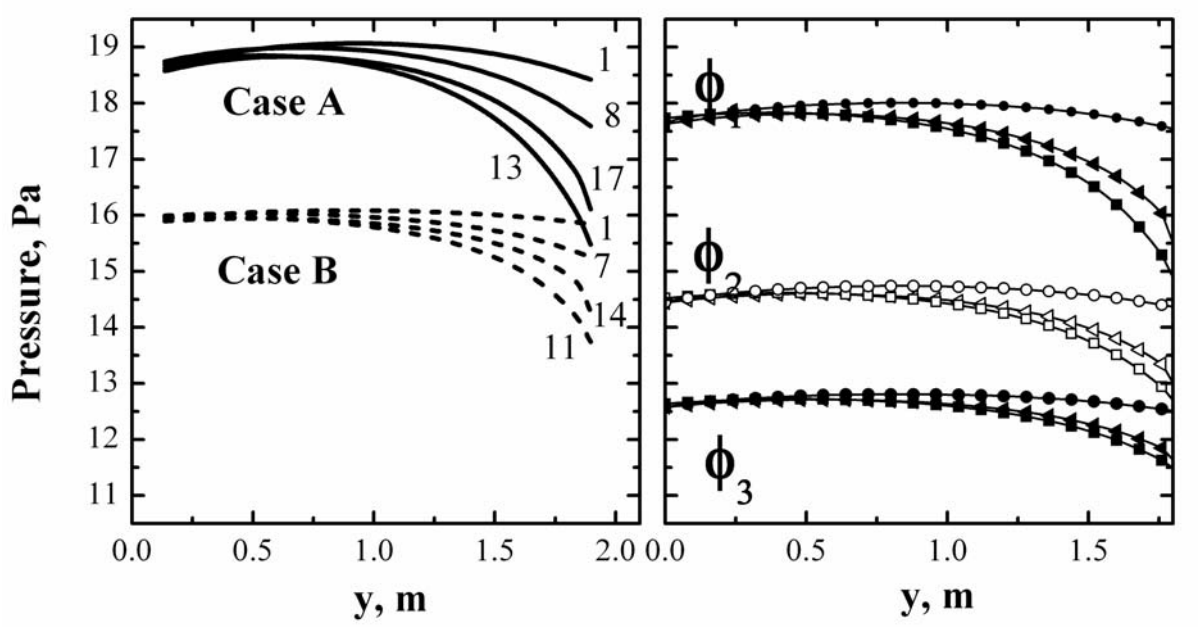
Pressure, Pa
19
18
17
16
15
14
13
12
11
Case A
Case B
1
8
13
17
1
7
14
11
0.0
0.5
1.0
1.5
2.0
y, m
ϕ
ϕ2
ϕ3
0.0
0.5
1.0
1.5
y, m

Figure 4

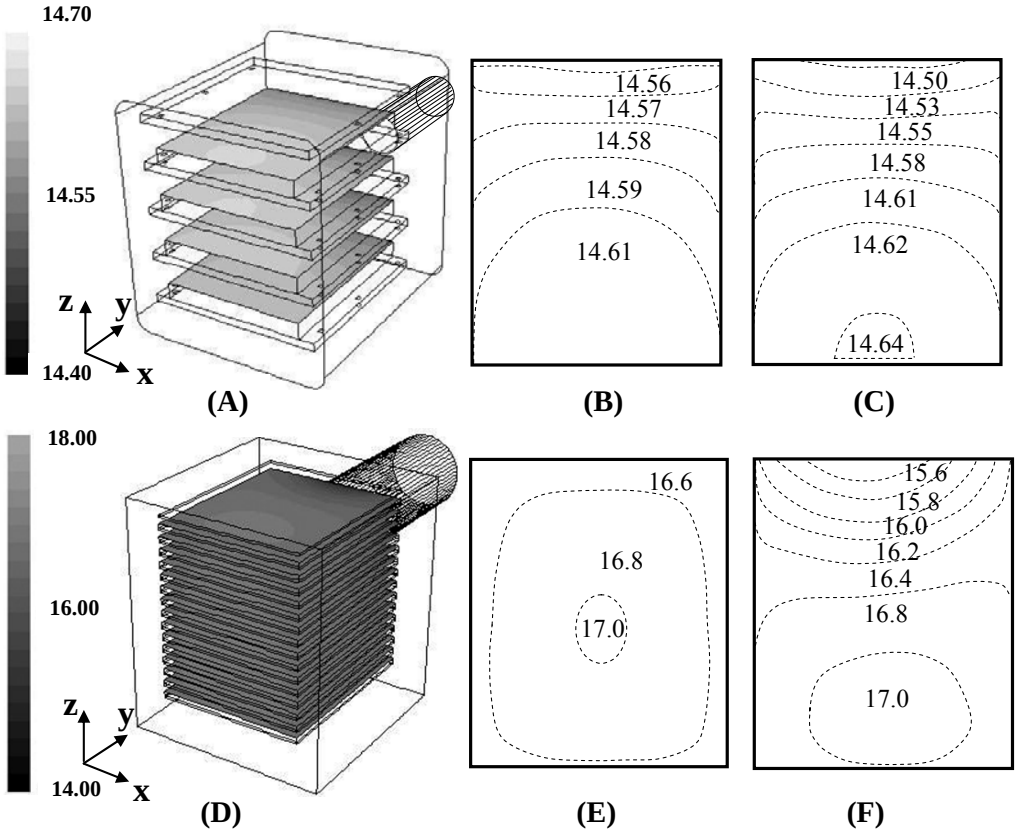
14.70
14.55
14.40
z
y
x
(A)
14.56
14.57
14.58
14.59
14.61
(B)
14.50
14.53
14.55
14.58
14.61
14.62
14.64
(C)
18.00
16.00
14.00
z
y
x
(D)
16.6
16.8
17.0
(E)
15.6
15.8
16.0
16.2
16.4
16.8
17.0
(F)

Figure 5

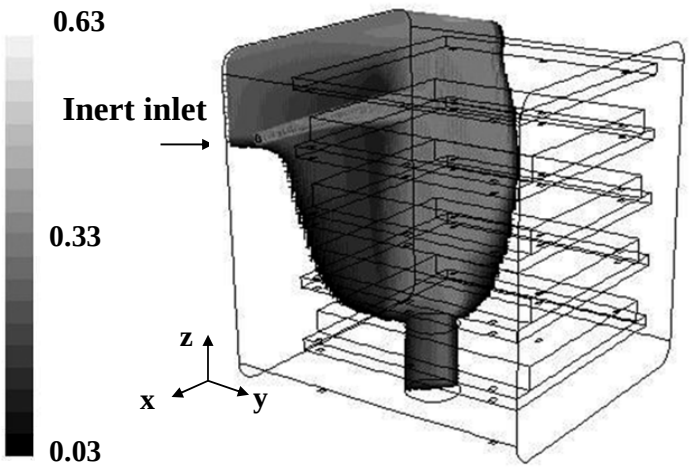

Figure 6

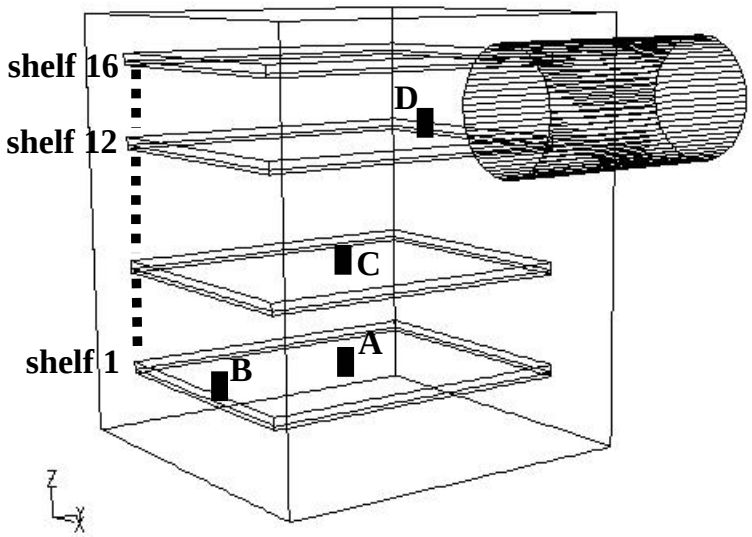

Figure 7

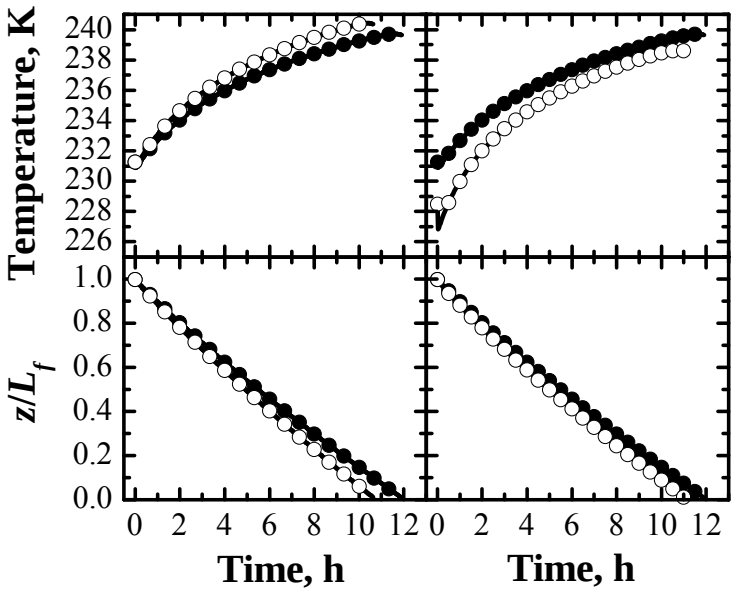
Temperature, K
240
238
236
234
232
230
228
226
z/L_f
1.0
0.8
0.6
0.4
0.2
0.0
0 2 4 6 8 10 12
Time, h
0 2 4 6 8 10 12
Time, h

Figure 8

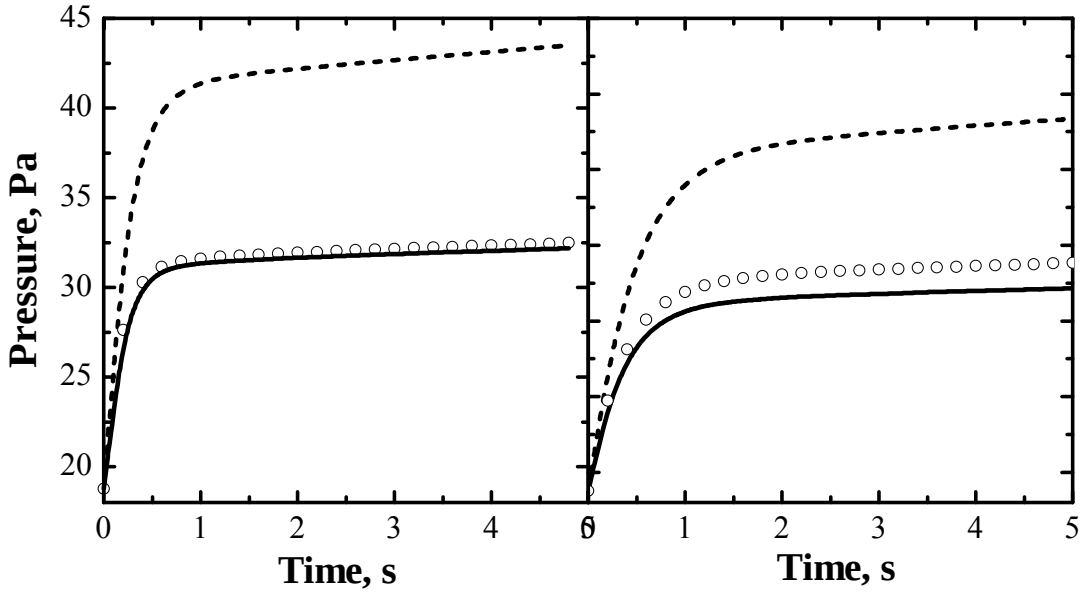

Figure 9

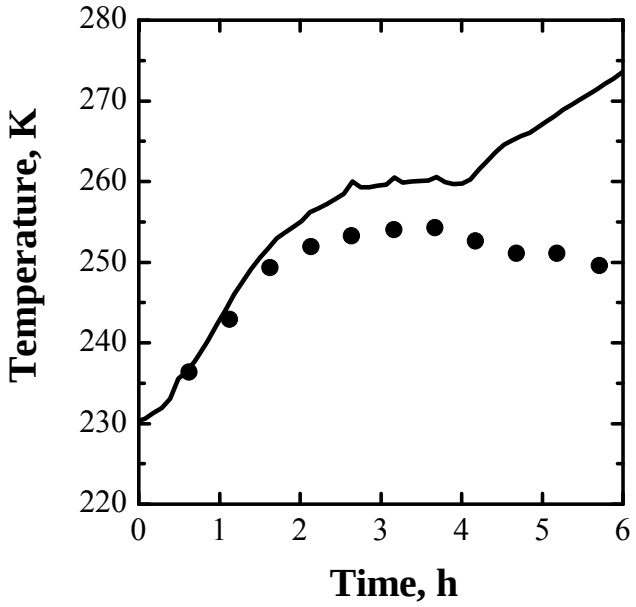

Figure 10